Optimal Selection of Motors and Transmissions in Back-Support Exoskeleton Applications

Erfan Shojaei Barjuei, M. Mahdi Ghazaei Ardakani, Darwin G. Caldwell, *Senior Member, IEEE*, Marcello Sanguineti, and Jesús Ortiz, *Member, IEEE*

***Abstract*—Because of the central role the actuator unit (electrical motors and transmission parts) has in wearable robots, improving the performance of the torque/force control system is vital, particularly for exoskeletons. This paper proposes an optimal approach to the selection of the main components of an actuation system (brushless DC motor and gearbox transmission) to be used in a back-support exoskeleton, but the principles can be extended and applied to other types of exoskeletons. To perform the optimization, an analytical model based on the dynamics of human–robot interaction has been developed. Moreover, to incorporate the weight of the actuator in the optimization framework, a mathematical relation between the weight and technical characteristics of the components, based on the polynomial regression technique using the low-discrepancy sequences method are developed. Consequently, the optimization criteria in terms of the closed-loop system frequency bandwidth, system power consumption and the weight of the components are formulated by imposing technical constraints on simulation parameters. The optimization results demonstrate two possible actuator combinations. Subsequently, the selected actuator components are evaluated in a lifting scenario by means of a linear quadratic regulator (LQR) controller with double integral action. Extensive simulation results in terms of the control frequency bandwidth, torque tracking control, current produced by motors and system robustness with respect to external disturbances are presented and discussed to make comparisons between the possible combinations of the components and their feasibility in the back-support exoskeleton applications.**

***Index Terms*—Wearable robots, exoskeletons, dynamic modeling, optimization, control frequency bandwidth, LQR.**

I. Introduction

RECENTLY, considerable research efforts have been devoted to the performance improvement of wearable robots such as exoskeletons [1]; although, the original study and investigation of exoskeletons can be traced back to at least 1890 [2]. Generally, an exoskeleton is a mechatronic system that is worn by a user to provide support and protection when performing physical tasks. It does this by generating appropriate assistive force(s) [3]. According to De Looze *et al.*, [4], a large group of workers are still requires to deal with physical workloads arising from load handling (more than 30% of workers in the EU). This issue has remained relatively stable over the past decade. Every year in the European Union, more than 40% of workers suffer from low back pain and shoulder pain. These statistics highlight the importance of the exoskeleton applications in industrial domains. Applications of exoskeletons can also be found in other domains such as military, medicine and rehabilitation [5]. An example of a back-support exoskeleton is shown in Fig. 1.

Unlike industrial robots, exoskeletons are designed to interact directly with the user. From a mechanical perspective, motion ranges, safety, wearer comfort, low inertia and adaptability should be considered, but at the same time, controllability, responsiveness, and flexible and smooth motion generation are also essential and form the core of any exoskeleton control system [6]. Therefore, optimization of these, often conflicting, demands is a challenge to the technological development of an exoskeleton. Basically, the performance of an exoskeleton as a robotic system depends on system parameters, operational tasks and robotic work-spaces [7], [8]. On this basis, the optimization problem has received substantial interest from researchers in several exoskeleton applications [9]–[13].

The combination of DC motors (often brushless) and gearbox transmissions (system actuator) provide the principal source of motion and force/torque in many exoskeleton systems [14]–[16], and this research aims to select an optimal combination of these components for a back-support exoskeleton [17]. In addition, from the control point of view, the elasticity (low stiffness) in exoskeleton systems, due to the contact environment (human body and elastic materials), reduces the closed-loop system frequency bandwidth [18].

Making the robotic system slow to respond to changes in the control parameters (torque in our case). That is, a higher control bandwidth frequency not only increases the potential of the robot control system to realize faster motion but also provides the possibility to compensate for dynamic effects and disturbances of external frequency contents [19]. Furthermore, mechatronic systems with low stiffness trend to have inefficient power transmission [20]. On this basis, the principal criteria of the optimization approach in this work are based

Manuscript received April 29, 2020; accepted July 8, 2020. Date of publication July 20, 2020; date of current version August 19, 2020. This article was recommended for publication by Associate Editor A. Knoll and Editor P. Dario upon evaluation of the reviewers' comments. This work was supported by the Italian Workers' Compensation Authority (INAIL). The work of Marcello Sanguineti was supported in part by CNR (National Research Council of Italy) under Project PDGP 2018/20 DIT.AD016.001 "Technologies for Smart Communities." *(Corresponding author: Erfan Shojaei Barjuei.)*

Erfan Shojaei Barjuei, Darwin G. Caldwell, and Jesús Ortiz are with the Advanced Robotic Department, Istituto Italiano di Tecnologia, 16163 Genova, Italy (e-mail: erfan.shojaei@iit.it; darwin.caldwell@iit.it; jesus.ortiz@iit.it).

M. Mahdi Ghazaei Ardakani is with the Department of Automatic Control, Faculty of Engineering, Lund University, 22100 Lund, Sweden (e-mail: mahdi.ghazaei@control.lth.se).

Marcello Sanguineti is with the Department of Computer Science, Bioengineering, Robotics, and Systems Engineering (DIBRIS), University of Genova, 16145 Genova, Italy (e-mail: marcello.sanguineti@unige.it).

Digital Object Identifier 10.1109/TMRB.2020.3010611

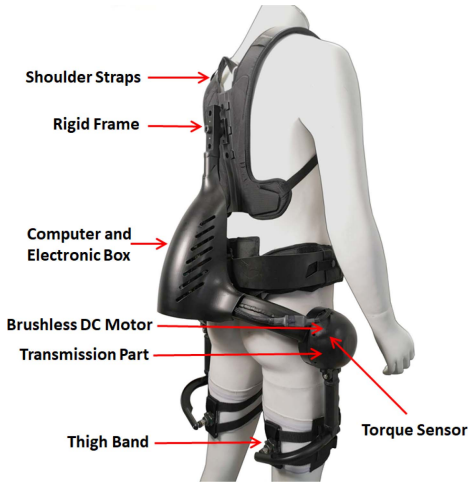

Fig. 1. Main components of a back-support exoskeleton.

on maximizing the closed-loop system frequency bandwidth. On the other hand, the system power consumption and weight of components act as constraints in the optimization approach. The development of a light-weight and low-energy consuming exoskeleton is an important challenge for the field of wearable robots since it can influence the cost, mobility, wearability, comfort, acceptance and maneuverability of the robotic platform. By way of illustration, Klein *et al.* in [21] developed an optimization algorithm for an exoskeleton framework to reduce the weight of the components. Furthermore, an important energy related problem associated with wearable robots is how to decrease the electrical power consumption (increasing energy efficiency), and limit the peak power (to improve user safety). As an example, Jatsun *et al.*, in [22] proposed to reduce the energy consumption of an exoskeleton by choosing the optimal time of the sit-to-stand motion (verticalization) in terms of the mechanism's energy consumption. However, optimization of energy usage in the combined motor-gearbox system generally requires a high gear-ratio that makes the system slow and unsuitable for force/torque and impedance control. One way to overcome this problem, which is basically correlated with the low frequency bandwidth of the system, is to take the frequency bandwidth into account in the optimization algorithm. This approach has been investigated and implemented in this work.

In [23] Rezazadeh and Hurst use the closed-loop system frequency bandwidth as one of the optimization objectives, however, control system stability as well as stiffness parameters, which have a strong effect on the system performance, are not included in their optimization criteria. With that being said, we have undergone a rethinking of the problem by extending the previous works to provide more details and more precise guidelines for selection and comparison of motors and their associated transmission systems in back-support exoskeleton applications. Accordingly, a more accurate dynamic model is developed and used to formulate, optimize, simulate and evaluate the overall system.

In this work, an optimization framework for the selection and evaluation of the main actuator components namely: the electric drive (brushless DC motor) and the associated transmission system (gearbox), for a back-support exoskeleton has been developed and presented. The approach in this work, aims to maximize the closed-loop system frequency bandwidth while constraining system power consumption, and the weight of physical components. These criteria are strongly dependent in the components, their configuration and size. To use the concept of frequency bandwidth in the optimization algorithm, a stable and robust closed-loop control system based on Youla-Kucera parametrization [24] has been formulated. Then, to incorporate the weight of the actuator into the optimization formulation, a mathematical relation between the component characteristics and their weights has been established using a polynomial regression technique based on the low-discrepancy sequences approach [25].

This paper expands and extends on the work published in [26] by improving the dynamic model and examining the performance of the final system through the simulation of a lifting task scenario that uses a linear quadratic regulator (LQR) controller with double integral action [27], instead of using a classical industrial controller (PID). Employing LQR control allows the designer to evaluate both the optimal setpoint tracking and optimal cost of the control within the same design framework. The work, described in this paper, features a novel and original optimization approach that has not been found in the scientific literature, based on the dynamics of human–robot interaction for exoskeleton applications.

This paper is organized as follows: first, the dynamic modeling of both the back-support exoskeleton and optimization objectives are described in Section II. In Section III, the optimization algorithm is formulated. The selection procedure as well as the performance analyses of possible combinations of components are discussed in Section IV. Finally, in Section V, conclusions are drawn.

II. The Dynamic Model

A. System Formulation

This section describes the synthesis of the analytical dynamic model of a back-support exoskeleton worn by a user. From this, a linear model is derived, which can be extended to any kind of upper-body exoskeleton. This increases the versatility of the approach.

When a person wears an exoskeleton, there are interaction forces that transfer energy between the user's body and the robot structure. The interaction forces can be modeled as a linear mass-spring-damper system, which is in fact also one of the approaches for the modeling of musculoskeletal systems [28]. In this approach, a limited number of masses represent the inertia properties of different segments of the human body including hard tissues and soft tissues. Springs and dampers represent the biomechanical properties of the different segments including bones, muscles, tendons, and ligaments.

To model the motion of the human trunk while wearing a back-support exoskeleton, a linear biomechanical model is illustrated in Fig. 2. The equivalent rotational stiffness,

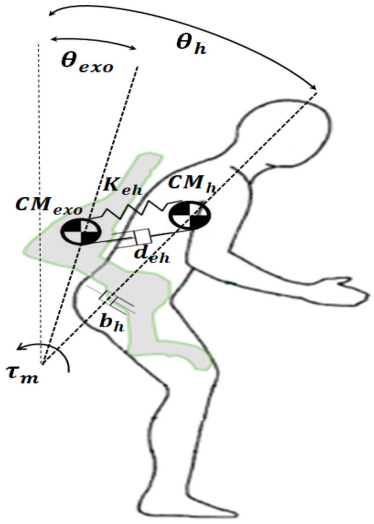

Fig. 2. Graphical representation of the sagittal plane of an upper-body exoskeleton and the operator based on the mass-spring-damper model.

including stiffness parameters between the human trunk and the exoskeleton, is represented by a rotational spring k_{eh} [N m rad^{-1}]. Similarly, the equivalent rotational damping between the human trunk and the exoskeleton is given by a rotational damper d_{eh} [N m s rad^{-1}]. The damping of the human hip, which corresponds to the rotation axis of the human upper-body, is represented by b_h [N m s rad^{-1}] and the center of mass locations of the human upper-body and the exoskeleton, relative to their axes of rotation, are given by CM_{hu} [m] and CM_{exo} [m], respectively.

It is assumed that the torque is applied to the operator's upper body (back) through a back-support exoskeleton (Fig. 2). This produces angular displacement θ_h [rad] with an angular velocity $\dot{\theta}_h$ [rad s^{-1}] and an angular acceleration $\ddot{\theta}_h$ [rad s^{-2}] of the human upper-body motion, as well as, angular displacement θ_{exo} [rad], angular velocity $\dot{\theta}_{exo}$ [rad s^{-1}] and angular acceleration $\ddot{\theta}_{exo}$ [rad s^{-2}] in the upper-body exoskeleton.

For clarity, a schematic model of a back-support exoskeleton is shown in Fig. 3. The model consists of a brushless DC motor with inertia J_m [kg m^2] coupled through the rotor to a strain wave gearbox with a gear-ratio of r_g and input inertia J_g [kg m^2] and damping b_g [N m s rad^{-1}]. The motor produces a torque τ_m, which results in the angular position being θ_m [rad], with a velocity of $\dot{\theta}_m$ [rad s^{-1}] and an acceleration of $\ddot{\theta}_m$ [rad s^{-2}]. The friction torque between the motor and the gearbox transmission is denoted by b_f [N m s rad^{-1}]. The stiffness k_g [N m rad^{-1}] and damping d_g [N m s rad^{-1}] of the gearbox transmission are modeled as parallel spring-damper elements. The torque sensor, mounted between the gearbox output and the rigid actuator link, is represented by a mass-spring-damper element with an internal ring inertia Js_{int} [kg m^2] and an external ring inertia Js_{ext} [kg m^2], stiffness k_s [N m rad^{-1}] and damping b_s [N m s rad^{-1}]. The positions of the internal ring and the external ring of the torque sensor are denoted by θs_{int} [rad] and θs_{ext} [rad], respectively. The human upper-body moment of inertia is represented by J_h [kg m^2]. Accordingly, the dynamic model of the system can be mathematically expressed as follows:

$$\tau_m - b_f\dot{\theta}_m - (J_m + J_g)\ddot{\theta}_m - \frac{k_g}{r_g}\left(\left(\frac{\theta_m}{r_g} - \theta s_{int}\right)\right) - \frac{d_g}{r_g}\left(\left(\frac{\dot{\theta}_m}{r_g} - \dot{\theta} s_{int}\right)\right) - \frac{b_g}{r_g}(\dot{\theta}_m) = 0 \quad (1)$$

$$k_g\left(\left(\frac{\theta_m}{r_g} - \theta s_{int}\right)\right) + d_g\left(\left(\frac{\dot{\theta}_m}{r_g} - \dot{\theta} s_{int}\right)\right) - Js_{int}\ddot{\theta} s_{int} - k_s(\theta s_{int} - \theta s_{ext}) - d_s(\dot{\theta} s_{int} - \dot{\theta} s_{ext}) = 0 \quad (2)$$

$$k_s(\theta s_{int} - \theta s_{ext}) + d_s(\dot{\theta} s_{int} - \dot{\theta} s_{ext}) - Js_{ext}\ddot{\theta} s_{ext} - k_{eh}(\theta s_{ext} - \theta_h) - d_{eh}(\dot{\theta} s_{ext} - \dot{\theta}_h) = 0 \quad (3)$$

$$k_{eh}(\theta s_{ext} - \theta_h) + d_{eh}(\dot{\theta} s_{ext} - \dot{\theta}_h) - J_h\ddot{\theta}_h - b_h\dot{\theta}_h = 0 \quad (4)$$

Furthermore, the velocity and acceleration of the internal torque sensor ring are denoted by $\dot{\theta} s_{int}$ [rad s^{-1}] and $\ddot{\theta} s_{int}$ [rad s^{-2}], respectively while the external torque sensor ring velocity is denoted by ($\dot{\theta} s_{ext}$ [rad s^{-1}]) and the acceleration is ($\ddot{\theta} s_{ext}$ [rad s^{-2}]).

B. Dynamic Model Simplification

Dealing with high-order dynamics systems such as exoskeletons with their complex computational schemes, creates very significant time and cost demands when dynamic performance analyses is required. Hence, a dynamic system simplification is presented in this section.

Generally, in mechatronics and robotics applications, when fast dynamics are required, systems with high efficiencies and low moments of inertia are preferred [29]. For simplification, the brushless DC motor and the gearbox transmission are assumed to have no loss. This assumption has also been used in other similar works such as [30]. It should be noted that the efficiency factor of the components will be taken into account during the selection procedure. Moreover, the friction torque between the motor and gearbox transmission (b_f) and the damping coefficients between the human body and exoskeleton (d_{eh}) are neglected as their values are so small in comparison with the those of the motor/gearbox and can easily be compensated. In our simplification, the torque sensor dynamics and its effects are also ignored since it is categorized as a measuring instrument and could be considered separately from the actuator unit.

Consequently, the dynamic model presented by equations (1-4) can be simplified to:

$$\tau_m - (J_m + J_g)\ddot{\theta}_m - \frac{k_{eh}}{r_g}\left(\frac{\theta_m}{r_g} - \theta_h\right) = 0 \quad (5)$$

$$k_{eh}\left(\frac{\theta_m}{r_g} - \theta_h\right) - J_h\ddot{\theta}_h - b_h\dot{\theta}_h = 0 \quad (6)$$

From equation (6), it is apparent that the torque applied on the human body is equal to the measured elastic torque and is equal to $k_{eh}(\frac{\theta_m}{r_g} - \theta_h)$.

C. Stable Controller Design

One of the main objectives that every feedback control system should satisfy is closed-loop stability [31]. The

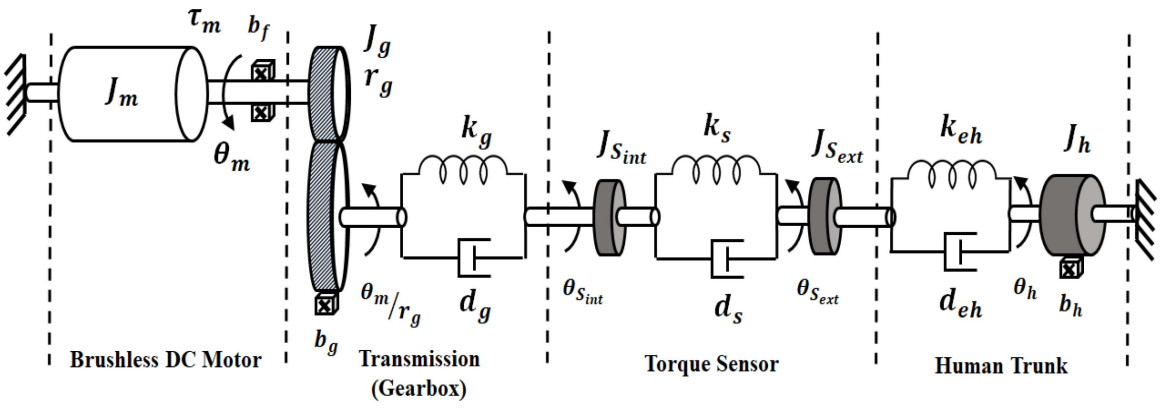

Fig. 3. Schematic representation of an exoskeleton system.

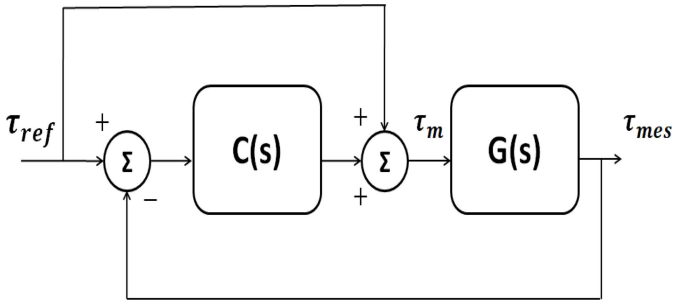

Fig. 4. Block diagram representation of a toque-controlled system for a back-support exoskeleton.

synthesis of a stabilizing controller based on Youla-Kucera parametrization, [32] is presented in this section.

The block diagram of a general toque-controlled back-support exoskeleton is shown in Fig. 4, where $G(s)$ and $C(s)$ represent the system and controller transfer functions, respectively. In Fig. 4, τ_{ref} is the reference torque, τ_{mes} denotes the torque applied on the human body and τ_m is the input torque (generated by the motor). Accordingly, the transfer function from τ_m to τ_{mes} can be written as:

$$G(s) = \frac{a_1 s + a_0}{b_3 s^3 + b_2 s^2 + b_1 s + b_0} \tag{7}$$

where,

$$a_0 = k_{eh} d_{eh} r_g \tag{8}$$
$$a_1 = J_h k_{eh} r_g \tag{9}$$
$$b_0 = k_{eh} d_{eh} \tag{10}$$
$$b_1 = \left(J_m + J_g\right) k_{eh} r_g^2 + J_h k_{eh} \tag{11}$$
$$b_2 = \left(J_m + J_g\right) d_{eh} r_g^2 \tag{12}$$
$$b_3 = J_h \left(J_m + J_g\right) r_g^2 \tag{13}$$

Taking (x, y) as Bézout's lemma coefficients [33] and knowing $\frac{x_0}{y_0} = 1$ ($x_0 = y_0$ is one particular possible solution) as a general stabilizing controller, one solution for the system transfer function in equation (7) to Bézout's equation can be given as:

$$\frac{b_3 s^3 + b_2 s^2 + b_1 s + b_0}{(s+1)^3} x + \frac{a_1 s + a_0}{(s+1)^3} y = 0 \tag{14}$$

Consequently, all stabilizing controllers for our system are possible solutions of equation (14):

$$\frac{y}{x} = \frac{1 - \frac{b_3 s^3 + b_2 s^2 + b_1 s + b_0}{(s+1)^3} q}{1 + \frac{a_1 s + a_0}{(s+1)^3} q} \tag{15}$$

in which, q is any proper stable rational function such that $1 + \frac{a_1 s + a_0}{(s+1)^3} q \neq 0$. By choosing $q = \frac{(s+1)^3}{b_3 s^3 + b_2 s^2 + b_1 s + b_0}$, one stabilizing controller can be obtained as:

$$C(s) = \frac{1}{b_3 s^3 + b_2 s^2 + b_1 s + a_1 s + b_0 + a_0 + 1} \tag{16}$$

To summarize, the controller presented in equation (16) can be used as a controller that guarantees the stability for our back-support exoskeleton framework.

D. Required Power

Peak power of a robot actuator is an important factor in setting the dimensions, cost and weight of the whole robotic system. The total motor power involves basically two parts: the electrical power losses in the motor and the mechanical losses in the components. Mathematically, the motor power can be expressed as follows:

$$P_m = P_{loss} + P_{mech} \tag{17}$$

in which, the motor losses (P_{loss}) are given by:

$$P_{loss} \approx R_m I^2 = R_m \frac{\tau_m^2}{K_t^2} \tag{18}$$

where K_t $[m\mathrm{N\,m\,A^{-1}}]$ represents the torque constant of the brushless DC motor. In equation (18), the approximation is based on the fact that magnetic and friction losses in brushless DC motor are small in comparison with resistive (R_m) losses. Moreover, the motor mechanical power (P_{mech}) is formulated as:

$$P_{mech} = \tau_m \dot{\theta}_m \tag{19}$$

As a consequence, the total motor power can be expressed as:

$$P_m = P_{loss} + P_{mech} \approx R_m \frac{\tau_m^2}{K_t^2} + \tau_m \dot{\theta}_m \tag{20}$$

By substituting τ_m into equation (20) from equations (5) and (6) and considering constant velocity ($\ddot{\theta}_h = 0$) for human motion. Equation (20) can be written as:

$$P_m \approx \left(\frac{R_m}{K_t^2} + \dot{\theta}_m\right)[k_{eh}^2\left(\frac{\theta_m}{r_g} - \theta_h\right)^2\left(\frac{r_g - 1}{r_g}\right)^2 + d_h^2\dot{\theta}_h^2 + 2k_{eh}\left(\frac{\theta_m}{r_g} - \theta_h\right)\left(\frac{r_g - 1}{r_g}\right) + d_h\dot{\theta}_h] \quad (21)$$

In equation (21), the terms associated with $(\frac{\theta_m}{r_g} - \theta_h)$ are very small since $(\theta_h/r_g \approx \theta_m)$. Therefore, by ignoring these terms, equation (21) can be simplified to:

$$P_m \approx \left(\frac{R_m}{K_t^2} + \frac{\dot{\theta}_h}{r_g}\right)\left[d_h^2\dot{\theta}_h^2 + d_h\dot{\theta}_h\right]. \quad (22)$$

The approximation of P_m according to equation (22) is used as an estimate of the total motor losses when developing the optimization algorithm in this work.

E. Weight of Components

Because we want to include the actuator weight in our optimization criteria, a mathematical model that relates the characteristics of the brushless DC motor, gearbox transmission and total weight of the combined actuator is required. Accordingly, the polynomial regression technique [34] is used to build a proper model. In fact, regression is a statistical measure that attempts to determine the strength of the relationship between one dependent variable and a series of other changing variables known as independent variables. The main advantages of using the polynomial regression respect to the linear one can be summarized as follows:

- Providing a better estimation for the relationship between the dependent and independent variable.
- Fitting a wider range of functions with a vast range of curvature.

The characteristics of the components, feasible and accessible for us, that can be technically applied on our back-support exoskeleton are collected. Accordingly, the information about the torque constant (K_t [mN m A^{-1}]) and gear-ratio (r_g) of available brushless DC motors and gearbox transmissions as well as their weight of their combination is reported in Table I. The first row and the first column of Table I describe the gear-ratio and the torque constant of available gearbox transmissions and brushless DC motors respectively. Hence, the resulting weight [g] of their combination is at the intersection of the corresponding row and column. It should be mentioned that the number of available and accessible components are limited and their distribution with respect to their features are not uniform. for this reason, feasible samples are generated in the modeling approach based on the low-discrepancy sequences technique which ensure a deterministic convergence at favorable rates when the number of sampling points grows [35], [36]. Random sampling methods, such as Monte Carlo sampling with a uniform distribution, result in points with a tendency to form clusters, particularly in high-dimensional contexts. The low- discrepancy sequences technique spreads these samples in a very uniform way so that the sample points are sufficiently close to one another, without leaving any region under-sampled.

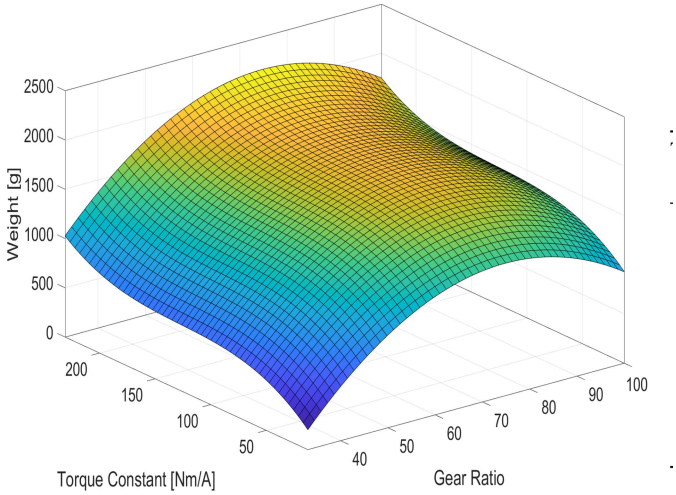

Fig. 5. 3D visualization of the polynomial model.

TABLE I
LOOK UP TABLE TO FIND THE ACTUATOR WEIGHT [g] BASED ON THE MOTOR TORQUE CONSTANT [mN m A^{-1}] AND GEARBOX GEAR RATIO

Torque Constant	Gear-Ratio							
	33	41	47	50	63	73	95	100
12.3	613	1073	613	278	1353	1953	1953	613
24.6	613	1073	613	278	1353	1953	1953	613
37.0	613	1073	613	278	1353	1953	1953	613
50.3	613	1073	613	278	1353	1953	1953	613
70.5	1060	1520	1060	725	1800	2400	2400	1060
109	1060	1520	1060	725	1800	2400	2400	1060
160	610	1070	610	275	1350	1950	1950	610
170	660	1120	660	325	1400	2000	2000	660
180	760	1220	760	425	1500	2100	2100	760
217	1060	1520	1060	725	1800	2400	2400	1060
231	1140	1900	1140	1105	2180	2780	2780	1140

Consequently, the mathematical model obtained from the polynomial regression can be expressed as:

$$\begin{aligned} W(K_t, r_g) = {} & 1714 + 366.3K_t + 43.91r_g - 356.4K_t^2 \\ & + \left(5.49 \times 10^{-14}K_t r_g\right) - 60.82r_g^2 \\ & + \left(7.07 \times 10^{-15}K_t^2 r_g\right) \\ & - \left(3.80 \times 10^{-14}K_t r_g^2\right) + 124.5r_g^3 \end{aligned} \quad (23)$$

Fig. 5 shows the 3D surface plot of the equation (23).

III. OPTIMIZATION PROBLEM

In this section, formulation of the optimization problem is introduced. The objective function to be maximized is the closed-loop frequency bandwidth *(BW)*, and constraints are imposed on the power consumption of the system and the actuator weight as:

$$\textit{Maximize} \quad BW\left(\frac{G(s)(C(s)+1)}{G(s)C(s)+r_g}\right) \quad (24)$$

subject to:

$$\left|\left(\frac{R_m}{K_t^2}+\frac{\dot{\theta}_h}{r_g}\right)\left[d_h^2\dot{\theta}_h^2+d_h\dot{\theta}_h\right]\right| \le U_{max}\frac{K_t}{R_m} \tag{25}$$

$$W\left(K_t, r_g\right) \le W_{act} \tag{26}$$

$$R_m, K_t, d_h, r_g, J_m, J_g, J_h, k_{eh} > 0, \quad \dot{\theta}_h \ Free \tag{27}$$

Equation (24) represents the objective function. The main idea behind this equation is to maximize the closed-loop system frequency bandwidth. In our case, the closed-loop frequency bandwidth is conventionally defined as the frequency at which the response of the system is reduced by 3 [dB] (half the power) from its maximum response. On the other hand, higher voltages provided by the power supply, result in higher torques being delivered at a certain speed. Accordingly, if the power supply cannot provide the required voltage, this causes a reduction in the motor current and the output torque as well. This fact has been implemented as a constraint in the optimization in inequality (25), where the right hand side is the maximum motor power and U_{max} is the maximum available motor voltage. That is 48 [V] in our case. Equation (25) defines the limitation on the actuator weight, formed by the sum of the weights of the brushless DC motor and gearbox. The maximum value is set to $W_{act} = 1$ [kg]. Furthermore, it is worth mentioning that all system parameters contain positive quantities; however, the value of $\dot{\theta}_h$ is arbitrary. This fact is implemented in equations (27).

The values of R_m, J_m and J_g are selected based on averaging values of available components in our database, i.e., $R_m \approx 0.85$ [Ω], $J_m \approx 2960$ [g cm^2] and $J_g \approx 0.285 \times 10^{-4}$ [kgm^2]. In the same way, the values of J_h, b_h and k_{eh} are estimated for a person of 1.75 [m] height and 75 [kg] weight based on information in [37], i.e., J_h, b_h and k_{eh} are set to 13.9 [kg m^2], 15.06 [N m s rad^{-1}] and 0.01 [N m rad^{-1}] respectively.

IV. Simulation Results and Selection Procedure

In this section the optimization results and the selection procedure are analyzed and discussed. The optimization method, used in this work, is based on constrained nonlinear optimization algorithms and it has been implemented in MATLAB software. It is worth mentioning that as our optimization algorithm is not based on ILP (Integer Linear Programming), the resulting outputs may not be integers. Hence, the closest, feasible components to the algorithm outputs will be evaluated and selected.

The optimization results suggest two sets of possible combinations of the gearbox transmission and bushless DC motor, namely:

- **Combination I:** A gearbox transmission with $r_g = 50$ and brushless DC motor with $K_t = 180$ [mN m A^{-1}]
- **Combination II:** A gearbox transmission with $r_g = 50$ and brushless DC motor with $K_t = 217$ [mN m A^{-1}]

Both combinations contribute to an actuator with a weight of less than 1 [kg], i.e., actuator combinations I and II are about 425 [g] and 725 [g] in weight, respectively. To assess the actuators performance, a simulation test has been carried out using a linear quadratic regulator (LQR) controller with double integral action. In this simulation, we assume that the back-support exoskeleton works in assistive mode. That is, a constant velocity ($\dot{\theta}_h = 0.1$ [rad s^{-1}]) for the user motion and a constant assistive torque that should be provided by the robot. This scenario is obtained by applying a step reference as the input with an amplitude of $\tau_{ref} = 20$ [N m] at 0.1 [s] for a period of 0.5 [s].

To perform the simulation tests, the values of b_f, b_g and d_g are estimated based on previous research [5] by the same authors, and are 0.48×10^{-3} [N s rad^{-1}], 0.65 [N s rad^{-1}] and 6 [N s rad^{-1}] respectively. We assume these values are the same for all components in our data set.

A. Synthesis of LQR With Double Integral Action

The theory described in the preceding sections allows assessment of both combinations I and II. The performance of the selected components has been evaluated through a closed-loop system by means of a LQR controller with a double integral action. Note that the design and implementation of the LQR control are not discussed here in details because it is not pertinent to the optimization algorithm. All the simulation results have been carried out using MATLAB/Simulink.

In order to implement a LQR controller, a linear time invariant (LTI) dynamic system must be available [38]. Therefore, the following state vector is taken into account:

$$x = [\theta_m \quad \dot{\theta}_m \quad \theta s_{int} \quad \dot{\theta} s_{int} \quad \theta s_{ext} \quad \dot{\theta} s_{ext} \quad \theta_h]^T \tag{29}$$

In fact, equations (1-4) can be reorganized and expressed in the matrix form as represented in equation (28), as shown at the bottom of the page. Accordingly, a more compact form

$$\begin{bmatrix} \dot{\theta}_m \\ \ddot{\theta}_m \\ \dot{\theta} s_{int} \\ \ddot{\theta} s_{int} \\ \dot{\theta} s_{ext} \\ \ddot{\theta} s_{ext} \\ \dot{\theta}_h \end{bmatrix} = \begin{bmatrix} 0 & 1 & 0 & 0 & 0 & 0 & 0 \\ \frac{-k_g}{(J_m+J_g)r_g^2} & \frac{-\left(b_f.r_g^2+b_g+d_g\right)}{(J_m+J_g)r_g^2} & \frac{k_g}{(J_m+J_g)r_g} & \frac{d_g}{(J_m+J_g)r_g} & 0 & 0 & 0 \\ 0 & 0 & 0 & 1 & 0 & 0 & 0 \\ \frac{k_g}{Js_{int}.r_g} & \frac{d_g}{Js_{int}.r_g} & \frac{-(k_g+k_s)}{Js_{int}} & \frac{-(d_g+d_s)}{Js_{int}} & \frac{k_s}{Js_{int}} & \frac{d_s}{Js_{int}} & 0 \\ 0 & 0 & 0 & 0 & 0 & 1 & 0 \\ 0 & 0 & \frac{k_s}{Js_{ext}} & \frac{d_s}{Js_{ext}} & \frac{-(k_{eh}+k_s)}{Js_{ext}} & \frac{-(d_{eh}+d_s)}{Js_{ext}} & \frac{k_{eh}}{Js_{ext}} \\ 0 & 0 & 0 & 0 & 0 & 0 & 0 \end{bmatrix} \times \begin{bmatrix} \theta_m \\ \dot{\theta}_m \\ \theta s_{int} \\ \dot{\theta} s_{int} \\ \theta s_{ext} \\ \dot{\theta} s_{ext} \\ \theta_h \end{bmatrix} + \begin{bmatrix} 0 & \frac{1}{J_m+J_g} & 0 & 0 & 0 & 0 \end{bmatrix}^T \tau_m + \begin{bmatrix} 0 & 0 & 0 & 0 & \frac{d_{eh}}{Js_{ext}} & 1 \end{bmatrix}^T \dot{\theta}_h \tag{28}$$

TABLE II
WEIGHTING MATRICES ASSOCIATED TO LQR CONTROLLER WITH DOUBLE INTEGRAL

Combination I	Combination II
$Q_c' = diag(10^5, 10^5, 10^7, 10^7, 10^7, 10^7, 5 \times 10^{13})$ $Q_c = diag(10^5, 10^5, 10^7, 10^7, 10^7, 10^7, 5 \times 10^{13}, 5 \times 10^{15})$ $R_c' = 5 \times 10^{10}$ $R_c = 5 \times 10^{10}$	$Q_c' = diag(10^5, 10^5, 10^7, 10^7, 10^7, 10^7, 5 \times 10^{13})$ $Q_c = diag(10^5, 10^5, 10^7, 10^7, 10^7, 10^7, 5 \times 10^{13}, 5 \times 10^{15})$ $R_c' = 4 \times 10^{11}$ $R_c = 4 \times 10^{11}$

of equation (28) can be expressed in the state-space form as follows:

$$\begin{cases} \dot{x}_1 = A_1 x_1 + A_3 x_2 + B_m \tau_m + B_{\dot{\theta}_{h_1}} \dot{\theta}_h \\ \dot{x}_2 = B_{\dot{\theta}_{h_2}} \dot{\theta}_h \\ y_x = H x_1 \\ y_b = C_b x_1 - k_{eh} x_2 - d_{eh} \dot{\theta}_h \end{cases} \tag{30}$$

where x_1 includes the first six states of x and x_2 and is equal to $\dot{\theta}_h$. $A_1 \in R^{6\times6}$ comprising the first six rows and columns of A, $A_3 \in R^{6\times1}$ containing the first six rows of the last column of A, $B_m \in R^{6\times1}$ consisting the first six rows of B_m, $B_{\dot{\theta}_{h_1}} \in R^{6\times1}$ including the first six rows of $B_{\dot{\theta}_h}$ and $B_{\dot{\theta}_{h_2}} \in R^{1\times1}$ and is equal to 1. Additionally, while $H \in R^{6\times6}$ is an identity matrix, the torque on the human body is denoted by y_b and can be formulated as a system output by setting C_b as:

$$C_b = \begin{bmatrix} 0 & 0 & 0 & 0 & k_{eh} & d_{eh} \end{bmatrix} \tag{31}$$

Hence, for an LQR controller with integral action, the following state-space equations are taken into account:

$$\underbrace{\begin{bmatrix} \dot{x} \\ \dot{z} \end{bmatrix}}_{\dot{x}_i'} = \underbrace{\begin{bmatrix} A_1 & 0_{6\times1} \\ -C_b & 0_{1\times1} \end{bmatrix}}_{A_i'} \underbrace{\begin{bmatrix} x \\ z \end{bmatrix}}_{x_i'} + \underbrace{\begin{bmatrix} B_m \\ 0 \end{bmatrix}}_{B_i'} \tau_m + \underbrace{\begin{bmatrix} B_{\dot{\theta}_h} \\ 0 \end{bmatrix}}_{B_h'} \dot{\theta}_h + \begin{bmatrix} 0 \\ 1 \end{bmatrix} \tau_{ref} \tag{32}$$

where τ_{ref} is the reference torque of the closed-loop control system and z is the auxiliary state corresponding to y_b. Thereby, the optimal state-feedback control law is obtained in the form:

$$u' = -F_i' x_i' = -F_{ix}' x - F_{iz}' z \tag{33}$$

where F_i' is the optimal feedback matrix gain, F_{ix}' represents the proportional matrix gain and F_{iz}' denotes the integral gain. Since $Q_c' \in R^{7\times7}$ and $R_c' \in R^{1\times1}$ are positive definite symmetric weighing matrices of LQR, the cost function which is associated with the system states the human velocity as the system input respectively. The location of the closed-loop poles are changed by varying the Q_c' and R_c' matrices, thereby changing the performance of the system. The larger elements of Q_c' causes faster convergence of the states. Similarly, large values of R_c' results in smaller control inputs and hence larger values of the states. The following specifications are used to obtain a suitable feedback matrix:

$$\begin{aligned} |\theta_m| &\le 0.001 \text{ [rad]}, \quad |\dot{\theta}_m| \le 0.002 \text{ [rad s}^{-1}\text{]} \\ |\theta s_{int}| &\le 0.0001 \text{ [rad]}, \quad |\dot{\theta} s_{int}| \le 0.0002 \text{ [rad s}^{-1}\text{]} \\ |\theta s_{ext}| &\le 0.0001 \text{ [rad]}, \quad |\dot{\theta} s_{ext}| \le 0.0002 \text{ [rad s}^{-1}\text{]} \\ |\tau_{m_1}| &\le 1.8 \text{ [N m]}, \quad |\tau_{m_2}| \le 1.0 \text{ [N m]} \end{aligned}$$

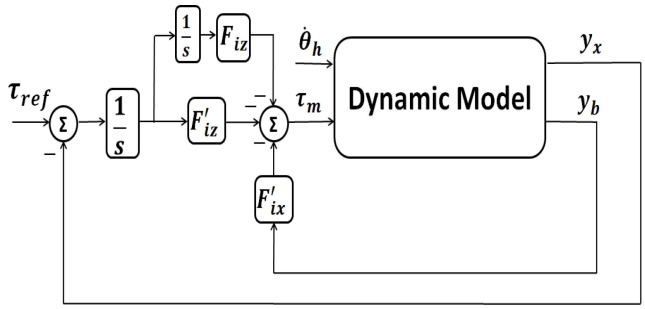

Fig. 6. Block diagram of the closed-loop control system based on a LQR with double integral.

where $|\tau_{m_1}|$ and $|\tau_{m_2}|$ are the nominal generated torque of the brushless DC motors in the first and second combinations respectively.

In order to reject ramp trajectories arising from the human trunk position when the human velocity is constant, LQR needs a double integral. Consequently, the following formulation is extracted:

$$A_i = \begin{bmatrix} A_1 & & & 0_{6\times2} \\ & -C_b & & 0_{1\times2} \\ 0 & 0 & 0 & 0 \quad 0 \quad 0 \quad 1 \quad 0 \end{bmatrix} \quad \text{and} \quad B_i = \begin{bmatrix} B_m \\ 0 \\ 0 \end{bmatrix} \tag{34}$$

The LQR optimal control law of equation (34) is obtained in the form:

$$u = -F_{ix}' x - F_{iz}' z - F_{iz} \int_0^t z d\tau \tag{35}$$

where t [s] is the instantaneous time and τ represents the variable of the integration corresponding to the time. The pair (A_i, B_i) is controllable and is a sufficient condition for the existence of a state feedback gain F_i such that $(A_i - B_i F_i)$ can be asymptotically stable. The controller matrix F_i is obtained from minimization of the quadratic performance index of the LQR controller for equation (34). The block diagram of the closed-loop control system is shown in Fig. 6, where the torque on the human body is indicated by y_b and F_{iz} is the gain related to the integral term associated with the torque on the human body (last array of F_i).

The resulting Q_c' and R_c' matrices and weighting matrices ($Q_c \in R^{8\times8}$ and $R_c \in R^{1\times1}$) associated with the LQR according to equation (34) for both combinations are reported in Table II. In addition, the computed state feedbacks for the controllers corresponding to combinations are shown in Table III.

TABLE III
STATE FEEDBACKS ASSOCIATED WITH LQR CONTROLLER WITH DOUBLE INTEGRAL

Combination I	Combination II
$F'_{ix} = [5.7\ 0.1\ 2.5\ 0.3\ 0.0\ 0.0]$ $F'_{iz} = [-14.1]$ $F_{iz} = [-316.2]$	$F'_{ix} = [2.6\ 0.0\ 0.6\ 0.0\ 0.1\ 0.0]$ $F'_{iz} = [-5.0]$ $F_{iz} = [-111.8]$

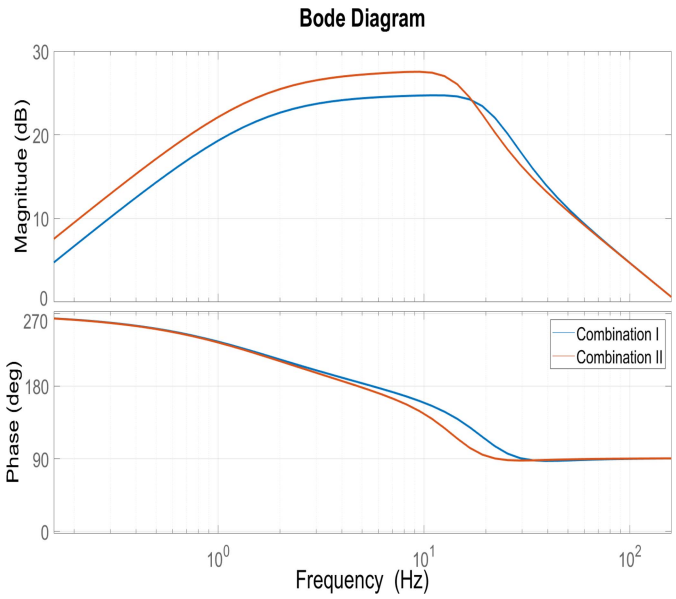

Fig. 7. Bode plots associated with the transfer function from the input disturbance (human velocity) to the torque on the human body.

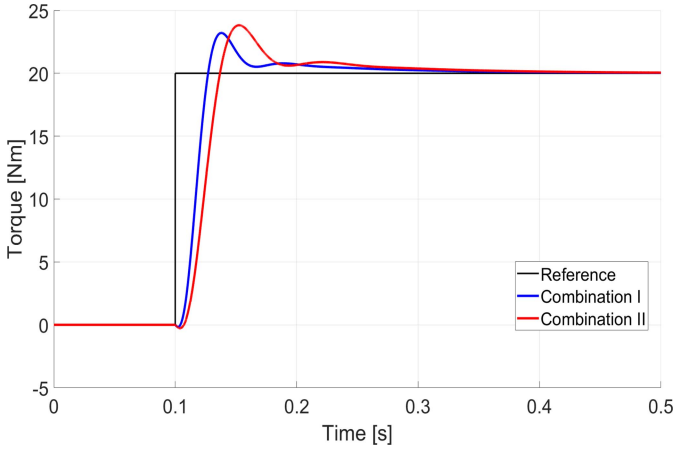

Fig. 8. Step response of the system for the torque on the human body.

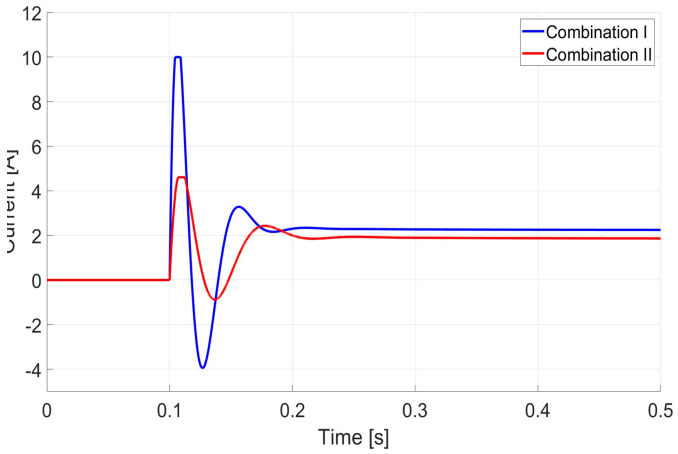

Fig. 9. Currents exerted by the brushless DC motors.

B. Performance Analysis

In this section, simulation tests to evaluate the performance of the exoskeleton with the selected components (brushless DC motor and gearbox transmission) are given and discussed.

To evaluate the disturbance rejection bandwidth, which means how fast the effects of human motion need to reduced to a level that is acceptable for the exoskeleton system, the bode plots of the transfer function from the input disturbance (human velocity) to the torque on the human body, for the both systems, are shown in Fig. 7. From the plots, it is clear that the disturbance (human velocity) to torque on the human body frequency responses, for the systems built using both combinations, are very similar. By defining the bandwidth as the frequency where the gain drops below -3 dB of its DC value, it can be inferred that the bandwidths for tracking disturbance (human velocity) rejection are near to 137 [Hz] and 103 [Hz] for combinations I and II, respectively; This is well above sufficient for human motion [39]. Moreover, the results provide evidence that the most detrimental effects on the torque appear in the frequency range of $\sim 6-11$ [Hz] for both cases.

Additional data on the systems performances are reported in Fig. 8, where a comparison is made between the step responses of the closed-loop control systems using the linear dynamic model. The performance analysis of the step response for each closed-loop control system, including actuators with combination I and II is reported in Table IV. This table provides a comparison of results on overshoot, undershoot, rise time, settling time and steady-state error. It should be mentioned that the slight undershoot at the beginning of the human motion is due to differences in the phase between the human velocity and the applied torque on the human body (non-minimum phase system).

The current plot during human motion, for two possible bushless DC motors ($K_t = 180$ [mN m A^{-1}] and $K_t = 217$ [mN m A^{-1}])]) in combination with a gearbox transmission with a gear-ratio of 50 during the human motion is illustrated in Fig. 9. The nominal current of each motor has been imposed as a constraint in the simulation. Furthermore, according to Fig. 9, the overall current produced by the motors, for both combinations, are within the defined current limit range, i.e., 10 [A] and 4.7 [A] for the first and second combination, respectively.

In order to analyze the robustness properties of the system with both actuator combinations, effects of an external disturbance on the measuring torque are studied and evaluated. Accordingly, a pulse of amplitude 2 [N] with a duration of 0.1 [s] is applied as a disturbance on the measurement of the torque signal (y_x). Fig. 10 demonstrates the effects of the external disturbance on the plant during the implementation of the assigned task. Hence, it can be inferred that both actuator

TABLE IV
PERFORMANCE ANALYSIS OF THE CLOSED-LOOP SYSTEM BASED ON ACTUATOR COMBINATIONS

Closed-loop system	Overshoot	Undershoot	Rise time	Settling time	Steady-sate error
Combination I	16.0%	0.9%	0.12 [s]	0.42 [s]	0.1 [N m]
Combination II	19.1%	1.4%	0.13 [s]	0.45 [s]	0.1 [N m]

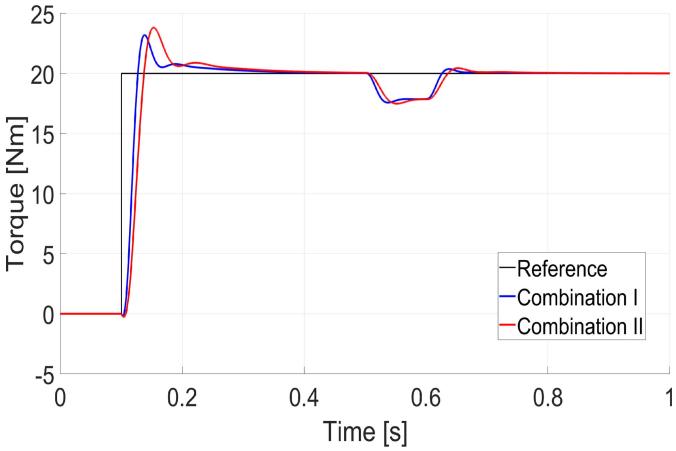

Fig. 10. Closed-loop system response of both combinations on the measuring torque in the presence of an external disturbance.

combinations are quite robust to such a disturbance. That is, the closed-loop system with both combinations have clearly attenuated the effect of the disturbance while retaining not only a precise tracking performance but also a good disturbance rejection.

From the short review above, the results demonstrated that both the actuator combinations perform similarly in terms of control frequency bandwidth and torque tracking control; however, the current produced by each actuator is different due to dissimilarities in the required power and technical constraints. Moreover, while the actuator combination I requires less current for an assigned lifting task that could fulfill better some safety standards, the weight of the actuator combination II weighs less that could have a better influence on the mobility and comfort of the exoskeleton. In this respect, as each application has its own unique characteristics and requirements, it is important to note which factor such as power, weight or efficiency is most important to the application. During this phase, the user may decide which actuator combination will better suit his needs.

V. CONCLUSION

In this paper, we present an approach for choosing the combination of a brushless DC motor and a gearbox transmission, to be used as the main actuator components in an industrial back-support exoskeleton. The work uses an analytical dynamic model based on the dynamics of human–robot interaction when wearing an exoskeleton. As a result, the formulation is more comprehensive than similar studies already reported in the literature, particularly as previously unmodeled stiffness parameters are incorporated into this new modeling approach. Principal among these are considerations that arise from the low stiffnesses associated with the non-linear viscoelastic properties of soft elements and the human body. These low stiffness characteristics can lead to reduced control bandwidths and inefficient power transmission.

Therefore, to improve the control performance, the closed-loop system frequency bandwidth is considered as the main optimization objective to be maximized. Subsequently, the models, which are derived for the weight of the components and power consumption of the system, are imposed as constraints in the optimization formulation. To make a mathematical model that relates the characteristics of the brushless DC motor and gearbox transmission, and the total weight of the resulting actuator, a polynomial regression technique based on the low-discrepancy sequences method is used to develop the optimization formulation.

As the optimization algorithms may propose different actuator combinations, the question of which components are best suited to use in back-support exoskeleton applications is difficult to answer analytically. To address this issue, evaluation testing was conducted to make a comparison between the performance of candidate components for specific tasks.

In this work, the frequency response associated with the human velocity as the system input to torque on the human body as the system output, torque tracking during bending at the waist (motion), current produced by brushless DC motors and the robustness properties of the system with respect to an external disturbance have been investigated during the system performance evaluation.The results from these simulations have been encouraging, and similar in terms of the closed-loop system frequency bandwidth and torque tracking control. In this sense the candidate actuator combinations can successfully fulfill the requirements of the assigned tasks; although, these actuator combinations are different with respect to their nominal current (power) and weight. Given this, to achieve the best combined motor-transmission solution, users should analyze their needs from different aspects such as: required power, allowed weight, cost, etc. This will help to ensure that they will receive the most effective solution that best suits the application.

Future developments of the work will aim to extend the optimization approach to other configurations of industrial exoskeletons such as shoulder-support exoskeletons. Furthermore, to extend the approach, additional constraints such motor stall torques and thermal limitations will be included in the optimization formulation to improve the evaluation and selection procedure.

ACKNOWLEDGMENT

The development of the exoskeleton technologies used in this work have been funded by the Italian Worker's Compensation Authority (INAIL). M. Sanguineti is a member

of GNAMPA-INdAM (Gruppo Nazionale per l'Analisi Matematica, la Probabilit'a e le loro Applicazioni - Istituto Nazionale di Alta Matematica).

REFERENCES

[1] S. Bai, G. S. Virk, and T. Sugar, *Wearable Exoskeleton Systems: Design, Control and Applications*. London, U.K.: Inst. Eng. Technol., 2018.

[2] E. Mikołajewska and D. Mikołajewski, "Exoskeletons in neurological diseases-current and potential future applications," *Adv. Clin. Exp. Med.*, vol. 20, no. 2, pp. 227–233, 2011.

[3] H. P. Crowell, J.-H. Park, C. A. Haynes, J. M. Neugebauer, and A. C. Boynton, "Design, evaluation, and research challenges relevant to exoskeletons and exosuits: A 26-year perspective from the U.S. army research laboratory," *IISE Trans. Occup. Ergonom. Hum. Factors*, vol. 7, nos. 3–4, pp. 199–212, 2019.

[4] M. P. De Looze, T. Bosch, F. Krause, K. S. Stadler, and L. W. O'Sullivan, "Exoskeletons for industrial application and their potential effects on physical work load," *Ergonomics*, vol. 59, no. 5, pp. 671–681, 2016.

[5] E. S. Barjuei, S. Toxiri, G. A. Medrano-Cerda, D. G. Caldwell, and J. Ortiz, "Bond graph modeling of an exoskeleton actuator," in *Proc. IEEE 10th Comput. Sci. Electron. Eng. (CEEC)*, Colchester, U.K., 2018, pp. 101–106.

[6] V. Kumar, Y. V. Hote, and S. Jain, "Review of exoskeleton: History, design and control," in *Proc. IEEE 3rd Int. Conf. Recent Develop. Control Autom. Power Eng. (RDCAPE)*, Noida, India, 2019, pp. 677–682.

[7] J. Solis, T. Sansanayuth, and E. Shojaei, "Velocity control improvement for the human-friendly assist robot vehicle," in *Proc. IEEE/SICE Int. Symp. Syst. Integr. (SII)*, Sapporo, Japan, 2016, pp. 331–336.

[8] J. Li *et al.*, "Magnetically-driven medical robots: An analytical magnetic model for endoscopic capsules design," *J. Magn. Mater.*, vol. 452, pp. 278–287, Apr. 2018.

[9] T. Poliero, S. Toxiri, D. G. Caldwell, and J. Ortiz, "Actuator optimization for a back-support exoskeleton: The influence of the objective function," in *Proc. Int. Symp. Wearable Robot.*, 2018, pp. 530–534.

[10] P. Malcolm, S. Galle, and D. De Clercq, "Fast exoskeleton optimization," *Science*, vol. 356, no. 6344, pp. 1230–1231, 2017.

[11] K. Mombaur, "Optimizing design characteristics of passive and active spinal exoskeletons for challenging work tasks," in *Proc. Wearable Robot. Challenges Trends Proc. 4th Int. Symp. Wearable Robot. (WeRob)*, vol. 22. Pisa, Italy, Oct. 2018, pp. 249–253.

[12] A. Zeiaee, R. Soltani-Zarrin, R. Langari, and R. Tafreshi, "Kinematic design optimization of an eight degree-of-freedom upper-limb exoskeleton," *Robotica*, vol. 37, no. 12, pp. 2073–2086, 2019.

[13] P. Yin, L. Yang, and B. Liu, "Design and optimization of a wearable upper limb exoskeleton based on adams," in *Proc. IOP Conf. Mater. Sci. Eng.*, vol. 717, 2020, Art. no. 012004.

[14] N. Karavas, A. Ajoudani, N. Tsagarakis, J. Saglia, A. Bicchi, and D. Caldwell, "Tele-impedance based assistive control for a compliant knee exoskeleton," *Robot. Auton. Syst.*, vol. 73, pp. 78–90, Nov. 2015.

[15] A. S. Koopman *et al.*, "The effect of control strategies for an active back-support exoskeleton on spine loading and kinematics during lifting," *J. Biomech.*, vol. 91, pp. 14–22, Jun. 2019.

[16] A. Zibafar, S. Ghaffari, and G. Vossoughi, "Achieving transparency in series elastic actuator of sharif lower limb exoskeleton using LLNF-NARX model," in *Proc. IEEE 4th Int. Conf. Robot. Mechatron. (ICROM)*, Tehran, Iran, 2016, pp. 398–403.

[17] D. Dresscher, T. J. de Vries, and S. Stramigioli, "Motor-gearbox selection for energy efficiency," in *Proc. IEEE Int. Conf. Adv. Intell. Mechatron. (AIM)*, Banff, AB, Canada, 2016, pp. 669–675.

[18] E. Rocon and J. L. Pons, *Exoskeletons in Rehabilitation Robotics: Tremor Suppression*, vol. 69. Berlin, Germany: Springer-Verlag, 2011, doi: 10.1007/978-3-642-17659-3.

[19] B. Laschowski, J. McPhee, and J. Andrysek, "Lower-limb prostheses and exoskeletons with energy regeneration: Mechatronic design and optimization review," *ASME J. Mech. Robot.*, vol. 11, no. 4, Aug. 2019, Art. no. 040801. [Online]. Available: https://doi.org/10.1115/1.4043460

[20] B. Laschowski, J. McPhee, and J. Andrysek, "Lower-limb prostheses and exoskeletons with energy regeneration: Mechatronic design and optimization review," *J. Mech. Robot.*, vol. 11, no. 4, 2019, Art. no. 040801.

[21] J. Klein, S. Spencer, J. Allington, J. E. Bobrow, and D. J. Reinkensmeyer, "Optimization of a parallel shoulder mechanism to achieve a high-force, low-mass, robotic-arm exoskeleton," *IEEE Trans. Robot.*, vol. 26, no. 4, pp. 710–715, Aug. 2010.

[22] S. Jatsun, S. Savin, and A. Yatsun, "Improvement of energy consumption for a lower limb exoskeleton through verticalization time optimization," in *Proc. IEEE 24th Mediterr. Conf. Control Autom. (MED)*, Athens, Greece, 2016, pp. 322–326.

[23] S. Rezazadeh and J. W. Hurst, "On the optimal selection of motors and transmissions for electromechanical and robotic systems," in *Proc. IEEE/RSJ Int. Conf. Intell. Robots Syst.*, Chicago, IL, USA, Sep. 2014, pp. 4605–4611.

[24] K. Zhou, J. C. Doyle, and K. Glover, *Robust and Optimal Control*, vol. 40. Upper Saddle River, NJ, USA: Prentice-Hall, 1996,

[25] A. Alessandri, C. Cervellera, and M. Sanguineti, "Design of asymptotic estimators: An approach based on neural networks and nonlinear programming," *IEEE Trans. Neural Netw.*, vol. 18, no. 1, pp. 86–96, Jan. 2007.

[26] E. S. Barjuei, M. M. G. Ardakani, D. G. Caldwell, M. Sanguineti, and J. Ortiz, "On the optimal selection of motors and transmissions for a back-support exoskeleton," in *Proc. IEEE Int. Conf. Cyborg Bionic Syst. (CBS)*, Munich, Germany, 2019, pp. 42–47.

[27] E. S. Barjuei and J. Ortiz, "A comprehensive performance comparison of linear quadratic regulator (LQR) controller, model predictive controller (MPC), H_∞ loop shaping and μ-synthesis on spatial compliant link-manipulators," *Int. J. Dyn. Control*, 2020. [Online]. Available: https://doi.org/10.1007/s40435-020-00640-z

[28] A. A. Nikooyan and A. A. Zadpoor, "Mass–spring–damper modelling of the human body to study running and hopping—An overview," *Proc. Inst. Mech. Eng. H, J. Eng. Med.*, vol. 225, no. 12, pp. 1121–1135, 2011.

[29] H. Giberti, S. Cinquemani, and G. Legnani, "A practical approach to the selection of the motor-reducer unit in electric drive systems," *Mech. Based Design Struct. Mach.*, vol. 39, no. 3, pp. 303–319, 2011.

[30] G. Cusimano, "Optimization of the choice of the system electric drive-device—Transmission for mechatronic applications," *Mech. Mach. Theory*, vol. 42, no. 1, pp. 48–65, 2007.

[31] E. S. Barjuei, P. Boscariol, R. Vidoni, and A. Gasparetto, "Robust control of three-dimensional compliant mechanisms," *J. Dyn. Syst. Meas. Control*, vol. 138, no. 10, 2016, Art. no. 101009.

[32] A. Paice and J. Moore, "On the Youla–Kucera parametrization for nonlinear systems," *Syst. Control Lett.*, vol. 14, no. 2, pp. 121–129, 1990.

[33] J. Pommaret and A. Quadrat, "Generalized bezout identity," *Appl. Algebra Eng. Commun. Comput.*, vol. 9, no. 2, pp. 91–116, 1998.

[34] Y.-W. Chang, C.-J. Hsieh, K.-W. Chang, M. Ringgaard, and C.-J. Lin, "Training and testing low-degree polynomial data mappings via linear SVM," *J. Mach. Learn. Res.*, vol. 11, pp. 1471–1490, Aug. 2010.

[35] A. Alessandri, C. Cervellera, D. Maccio, and M. Sanguineti, "Optimization based on quasi-monte carlo sampling to design state estimators for non-linear systems," *Optimization*, vol. 59, no. 7, pp. 963–984, 2010.

[36] R. Zoppoli, M. Sanguineti, G. Gnecco, and T. Parisini, *Neural Approximations for Optimal Control and Decision*. Cham, Switzerland: Springer, 2020, doi: 10.1007/978-3-030-29693-3.

[37] M. M. Catalá, A. Schroll, G. Laube, and A. Arampatzis, "Muscle strength and neuromuscular control in low-back pain: Elite athletes versus general population," *Front. Neurosci.*, vol. 12, p. 436, Jul. 2018.

[38] E. S. Barjuei, P. Boscariol, A. Gasparetto, M. Giovagnoni, and R. Vidoni, "Control design for 3D flexible link mechanisms using linearized models," in *Advances on Theory and Practice of Robots and Manipulators*. Cham, Switzerland: Springer, 2014, pp. 181–188. [Online]. Available: https://doi.org/10.1007/978-3-319-07058-2_21

[39] F. Bianchi *et al.*, "Localization strategies for robotic endoscopic capsules: A review," *Exp. Rev. Med. Devices*, vol. 16, no. 5, pp. 381–403, 2019.

Erfan Shojaei Barjuei received the bachelor's degree in electrical engineering from Azad University, Iran, in 2006, the master's degree in mechatronics engineering from the Sharif University of Technology, Iran, in 2008, and the Ph.D. degree in industrial and information engineering from the University of Udine, Italy, in 2016. He is currently a Postdoctoral Researcher with the Department of Advanced Robotics, Italian Institute of Technology. His research interests include modeling and control of mechatronic systems.

M. Mahdi Ghazaei Ardakani received the M.Sc. degree in secure telecommunication from the Department of Electrical Engineering, Iran University of Science and Technology, in 2006, the master's degree in robotics and intelligent systems from Örebro University, Sweden, in 2011, and the Ph.D. degree from the Department of Automatic Control, Lund University, Sweden, in 2016. He was a Postdoctoral Researcher with the Department of Advanced Robotics (ADVR), Istituto Italiano di Tecnologia. His research interests include robotics, system and control theory, and machine learning.

Darwin G. Caldwell (Senior Member, IEEE) received the B.Sc. degree in robotics from the University of Hull in 1986, the M.Sc. degree in management from the University of Salford, in 1994, and the Ph.D. degree in robotics from the University of Hull in 1990. From 1989 to 2006, he was with the University of Salford as a Lecturer, a Senior Lecturer, and a Reader, becoming a Full Professor of advanced robotics in 1999. He is an Honorary Professor with the University of Manchester, the University of Sheffield, the University of Bangor, and Kings College London in the U.K., and Tianjin University and the Shenzhen Academy of Aerospace Technology in China. In 2015, he was elected a Fellow of the Royal Academy of Engineering.

Marcello Sanguineti received the *Laurea* (M.Sc.) degree in electronic engineering and the Ph.D. degree in electronic engineering and computer science from the University of Genova, Italy, where he is currently an Associate Professor (Full Professor since November 1, 2020) of operations research. He is also a Research Associate with the Institute for Marine Engineering (INM), National Research Council of Italy (CNR). He coauthored more than 200 research papers in archival journals, book chapters, and international conference proceedings. His main research interests are infinite-dimensional programming, machine learning, neural networks for optimization, network and team optimization, affective computing, and game-theoretical models.

Jesús Ortiz (Member, IEEE) received the M.Sc. degree in mechanical engineering and the Ph.D. degree in new automobile technologies from the University of Zaragoza in 2003 and 2008, respectively. Since 2006, he has been working with the Istituto Italiano di Tecnologia and he is currently the Leader of the exoskeletons group (XoLab), Department of Advanced Robotics (ADVR). He has participated in six European projects, being the Coordinator of the XoSoft EU Project. He has over 60 international publications. His principal research field is industrial exoskeletons and soft wearable assistive devices. Previous research experience includes motion bases, driving simulators, teleoperation, telepresence, teleexistence, virtual reality, GPGPU computing, and medical robotics.